Collisions, adsorption and self diffusion of gas in nanometric channels by Molecular Dynamics and stochastic simulation and the case of Helium gas in graphitic slit pore

Pierre Magnico, Quy-Dong To

Collisions, adsorption and self diffusion of gas in nanometric channels by Molecular Dynamics and stochastic simulation and the case of Helium gas in graphitic slit pore

Pierre Magnico[a], Quy-Dong To[b,*]

[a] *Aix Marseille Univ, CNRS, Centrale Marseille, M2P2 UMR 7340, 13451 Marseille, France*
[b] *Univ Gustave Eiffel, Univ Paris Est Creteil, CNRS, UMR 8208, MSME, F-77454 Marne-la-Vallée, France*

Abstract

We investigate and model the collisions and the self diffusion processes of dilute Helium gas in nanometric graphite channels using molecular dynamics. At high temperature, collisions are mostly specular with short resident time. At temperature as low as 50 K-75 K, the gas atoms stay longer near the surface and the surface diffusion becomes dominant. Both ballistic and diffusive transport regimes are present before the desorption. A waiting time model based on the residence time distribution and coupled with ballistic-diffusive surface motion of atoms and with Cercignani-Lampis scattering model is proposed. The stochastic simulation of self diffusion based on the waiting time model agrees with the MD simulations and theoretical results in literature. The Arrhenius law is used to model the variation of the obtained Knudsen diffusivity as functions of temperature.

Keywords: Molecular Dynamics, gas wall collisions, accommodation coefficient, adsorption, Knudsen diffusion, surface diffusion.

*Corresponding author. Email: quy-dong.to@univ-eiffel.fr (Quy-Dong To), pierre.magnico@univ-amu.fr (Pierre Magnico)

1. Introduction

Gas transfer through nanochannel belongs to class of problems characterized by high Knudsen number and high specific surface. It concerns numerous industrial applications. In particular graphene or graphite materials are used for gas sensors [1, 2, 3], heterogeneous catalysis [4, 5], gas separation [6, 7, 8], fuel cell [9, 10, 11, 12], shale gas [13, 14, 15] reservoirs. Owing to its specific thermodynamic properties, Helium is widely used for cryogenics, chromatography, welding, breath mixture for instance [16, 17, 18]. As the channel width decreases to nanoscale, the gas mean free path becomes larger than the channel size and the gas/gas collisions become negligible compared to the collisions with the channel surface. In this case the gaseous medium cannot be considered as continuous and transport properties such as Knudsen diffusion are mainly sensitive to the gas/wall interaction. In particular, velocity slip and temperature jump at the wall surface are controlled by the gas/wall collision mechanisms [19, 20, 21, 22]. Therefore, an accurate knowledge of the surface structure (e.g crystalline plane, impurities, roughness, physicochemical gas/wall interaction) is necessary to predict the gas/wall energy and momentum transfer.

The Maxwell scattering model [23] assumes that the gas/wall collisions is either diffusive or is specular and the fraction of diffuse collision is called the accommodation coefficient. In case of very dilute gas, the mass transfer is considered as a series of free flights between collisions with the channel surface. The self diffusivity is theoretically derived by Knudsen [24] using purely diffusive wall and Smoluchowski [25] using Maxwell model. It is known that the simplicity of the Maxwell model does not capture well the collision behavior of atoms, compared with more sophisticate Cercignani-Lampis (CL) scattering kernel [26]. The latter is a smooth kernel in probability space, constructed from two parameters, a tangential momentum accommodation coefficient α_t (TMAC) and a normal energy accommodation coefficient α_n (NEAC). Arya et al. [27] extended the Smoluchowski results with CL kernel,

showing a good agreement with MD simulations of Knudsen diffusion in slit rigid pores. Liang et al. [28, 29] used a washboard model [30] but like the previous work, the rigid pores model are adopted and the adsorption is not considered.

When the gas atoms strike the pore surface, they can bounce several times before leaving the surface or scatter back [31, 32]. In the first case, the atoms remain bounded to the surface as long as the normal kinetic energy is lower than the surface potential well depth and the velocity correlation decreases with the bounce number [29, 32]. For the directly scattered atom, the incident and the reflected velocities are strongly correlated, especially when the roughness is small and the collision is elastic. As the temperature T decreases, the resident time increases and the velocities are less correlated. The motion of the adsorbed atoms can be viewed as surface diffusion and modelled by the Langevin equation [33, 34, 35, 36]. The time dependent means square displacement (MSD) can be characterized by transition from the ballistic to the diffusion regime. In some systems at small temperature, the Arrhenius law may be observed [37, 38].

To model the collision behavior which can be used to simulate gas transport in general and Knudsen diffusion process in particular, TMAC is determined from the correlation between the incoming and the outgoing velocity [28, 39]. At small temperature range, TMAC reflects the adsorption process and is more sensitive to temperature. At high temperature range, TMAC is less sensitive to temperature as the roughness effects dominates. To our knowledge, few studies are devoted to obtain the general relation of TMAC in terms of temperature [40, 41, 42, 43, 44]. Similarly, while the Knudsen diffusion is expected to depend on the temperature via the coefficient TMAC, the link between the Knudsen diffusion to the bulk and surface diffusion must be investigated [45, 46, 47, 48, 49, 50]. While some theoretical works [46, 51]

are based on purely diffusive surface mass transfer, from MD simulation of helium, we find that the ballistic regime in certain temperature range must also be taken into account.

The goal of the present work is to investigate the influence of surface diffusion, TMAC and the Knudsen diffusion on the self diffusion of gas in nanochannel over a large temperature range. To this end, we consider the system composed of graphene slit pore and helium gas in thermal equilibrium. Owing to the nanoscale of the system and of the gas/wall interaction, molecular dynamics (MD) is used in this study. We find a large TMAC variation and the diffusivity over the temperature range investigated and the adsorption and the surface roughness effects dominates in two different temperature regions. While the atomic surface can viewed as perfectly smooth from the average atom positions, the potential energy surface and the thermal motion of the atoms contribute to the roughness of the surface.

The results are presented as follows. In section 2, the gas/wall collision process is analyzed via the accommodation parameters and then the surface diffusion mechanism is described over the temperature range investigated. Residence time distribution, transition from ballistic to classical diffusion regime and time correlation are examined. From these results, stochastic models of Knudsen diffusion are developed and compared to the MD results in section 3 and theoretical results [27]. In section 4, the self diffusion in nanochannel is investigated via the time dependent mean square displacement (MSD) and we also observed the transition from short time ballistic to long time diffusive regime. The evolution of the transition time with temperature T agrees with the MD results. This parameter combined with the diffusion coefficient allows to define a normalized quantity which shows clearly the surface mass transfer transition from small temperature to high temperature.

2. Gas-wall interactions

2.1. Wall and gas atomic models and interaction potential

All molecular dynamics (MD) simulations involving graphite constituted of Carbon atoms (C) and Helium (He) gas atoms are performed with LAMMPS (Large-scale Atomic Molecular Massively Parallel Simulator) package. The adaptive intermolecular reactive bond order (AIREBO) potential is used for the interaction between the graphite carbon atoms. The 12-6 Lennard Jones (LJ) potential is used to model interaction between carbon and helium atoms :

$$V_{HeC} = 4\epsilon_{HeC}\left[\left(\frac{\sigma_{HeC}}{r}\right)^{12} - \left(\frac{\sigma_{HeC}}{r}\right)^{6}\right] \tag{1}$$

with $\sigma_{HeC} = 3$ Åand $\epsilon_{HeC} = 0.0015$ eV [52, 53, 54]. Instead of using classical cutoff distance $2.5\sigma_{HeC}$ in most MD simulations of LJ fluids, it is suggested that a larger cutoff distance r_{cut} should be used to model accurately the adsorption [55]. Separate tests on the sensitivity of r_{cut}, show that between 12 Å and 24 Å, the variation of accommodation coefficient is less than 5%. For the rest of the present work, the value $r_{cut} = 4\sigma_{HeC} = 12$ Å, which has reasonable computation cost and good accuracy, will be adopted.

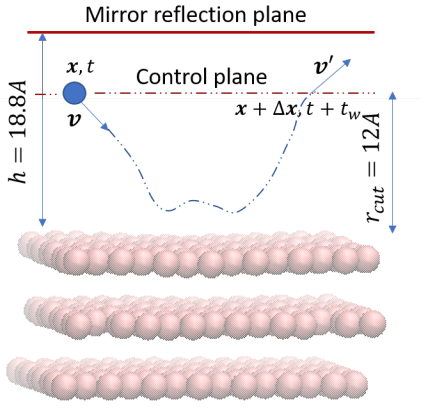

Figure 1: Illustration of collision simulations

The wall model is composed of 3 graphene layers with dimensions 17.04 Å$\times$ 17.22 Å in the plane xOy and is periodic in x and y directions. The wall contains 336 carbon atoms and has a width of 6.8 Å. During the simulation, the lowest sheet is fixed and the two others are maintained at constant temperature T by Nosé-Hoover thermostat in the NVT ensemble with the relaxing temperature parameter equals to 40 time steps. The layers are free to interact with the He atoms. About 1×10^6 time steps of 1 fs are devoted to equilibrate the system at the desired temperature before proceeding the next statistics steps. The velocity-Verlet algorithm is used for time integration.

2.2. Gas-wall interaction statistics

Since the diffusion in nanopore involves interaction between gas atoms and wall, we carry out a separate study of gas/wall collision statistics at different temperature T ranging from 50 K to 750 K (see Fig. 1). In the study, a graphitic wall serves as the lower boundary and a reflective plane at distance 18.8 Å from the surface as the upper boundary. A control plane is placed at distance $z_p = r_{cut}$ from the carbon surface where we records information of crossing atoms including incoming/outgoing time, velocities and their displacements during the resident time. The latter is the time the atoms spent within the cutoff distance z_p, equivalent to the time stamp difference between outgoing and incoming events. About 40000 collisions are collected for each temperature case T. Similar design of the numerical experiments can be found in previous works [56, 57, 58].

To examine the statistical relation between the incident atoms and reflected atoms, we look first at the correlation map of the collision data (Fig. 2). By definition, the correlation coefficient ρ_{AB} between A and B is

$$\rho_{AB} = \frac{cov(A, B)}{\sigma_A \sigma_B} \tag{2}$$

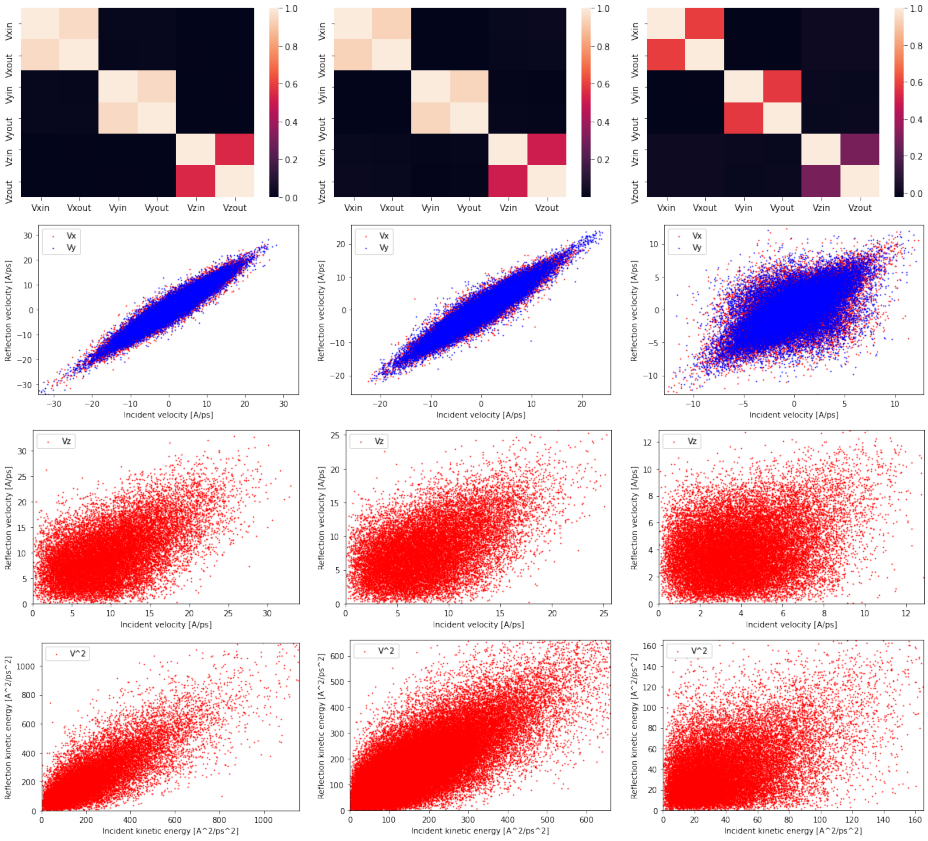

Figure 2: Collision data at 350 K (left column), 200 K (center column) and 50 K (right column). Top row: correlation map of incident and reflected velocity components. Second row: Scatter plot of incident and reflected velocity v_x, v'_x and v_y, v'_y. Third row: Scatter plot of incident and reflected velocity v_z, v'_z. Bottom row: Scatter plot of incident and reflected energy v^2, v'^2

where $cov(A, B)$ is the covariance and σ_A and σ_B the standard deviation of the two quantities A, B. Here A, B are any functions of the incident velocity components v_x, v_y, v_z and the reflected velocity components v'_x, v'_y, v'_z. We note that the correlation coefficient can also be used to determine accommodation coefficients in different gas-wall scattering kernels, Cercignani-Lampis or Maxwell models [23, 26, 28]. For example, the accommodation coefficients $\alpha_{AA'}$ for incident quantity A and the reflected quantity A' is given by the expression

$$\alpha_{AA'} = 1 - \rho_{AA'} \tag{3}$$

Of all the accommodation coefficients, we are interested in three parameters: tangential momentum accommodation coefficient (TMAC) $\alpha_{v_x v'x}$, or shortly α_t, normal momentum accommodation coefficient (NMAC), or shortly $\alpha_{v_z v'_z}$ or α_n and energy accommodation coefficient (EAC) $\alpha_{v^2 v'^2}$, or shortly α_e.

For all considered temperature, the correlation map show a strong correlation between the velocity of the same type (same direction), i.e v_x vs v'_x, v_y vs v'_y and v_z vs v'_z and weaker correlation between velocity of different directions, e.g v_x vs v'_y. This suggests that the reflected mechanism of each directions x, y, z may be independent. To investigate in detail the statistical relation v_x vs v'_x, v_y vs v'_y, v_z vs v'_z and v^2 vs v'^2, we do the scatter plot of incident and reflected velocities (see Fig. 2). From the first observation, we find that the form of collision data population changes from high to small temperature. The surface can be considered as isotropic as the data of (v_x, v'_x) and (v_y, v'_y) have the same form and correlation parameters. At high temperature $T = 350$ K, the data (v_x, v'_x) and (v_y, v'_y) is more centralized at the vicinity of a straight line, meaning the reflection is close to specular and the correlation coefficient close to 1 with $\rho_{v_x v'_x} = \rho_{v_y v'_y} = 0.955$ (or $\alpha_t = 0.045$). The same remark can be made for the energy as it exhibits nearly elastic collision and

small α_e value. Regarding the normal velocity (v_z, v'_z), the specular effect is less pronounced as the data is less localized than the tangential velocity. At low temperature as $T = 50$ K, the data is much more scattering, or the reflection is more diffusive and $\rho_{v_x v'_x} = \rho_{v_y v'_y} = 0.58$ (or $\alpha_t = 0.42$).

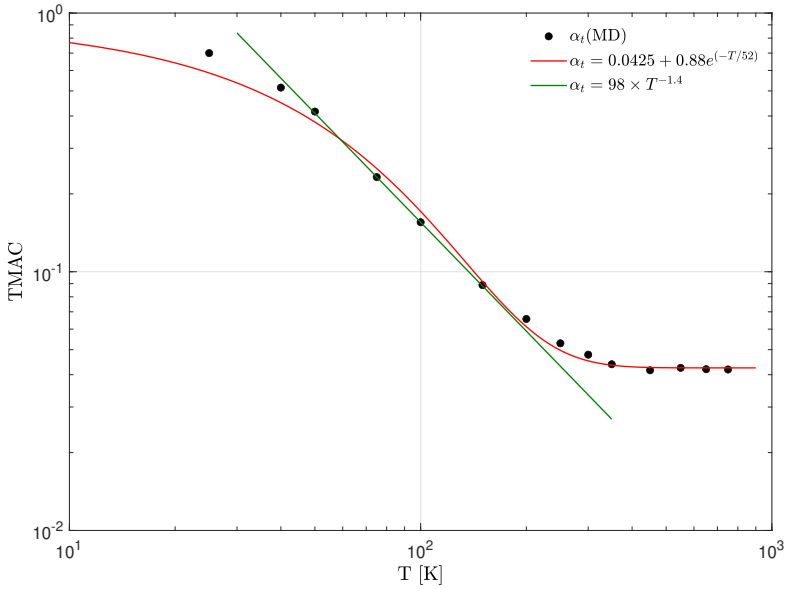

Figure 3: TMAC (α_t) vs. temperature. (•) : TMAC computed by molecular dynamics. Solid lines: fitting functions.

Figure 3 shows the temperature dependence of α_t. As suggested by Cao et al. [40], the TMAC can be estimated with the exponential expression:

$$\alpha_t(T) = \alpha_\infty + \alpha_0 e^{-\frac{T}{T_0}} \tag{4}$$

where α_∞ and α_0 are the TMAC at high temperature and the TMAC variation amplitude respectively. The temperature T_0 is related to the gas/wall interaction intensity, i.e the well depth of the LJ potential and α_∞ reflects the wall roughness at high temperature. Considering that at very small temperature, the collision must be diffusive owing to the adsorption effect, α_∞

and α_0 are linked to the following constraint:

$$\alpha_\infty + \alpha_0 = 1 \tag{5}$$

The three parameters α_∞, α_0 and T_0 are determined by fitting (4) with MD results in the temperature range of investigation 50K-750 K. In these cases, their values are $\alpha_\infty \simeq 0.0425$ and $\alpha_0 \simeq 0.88$ and characteristic temperature $T_0 \simeq 52$K and $\alpha_0 + \alpha_\infty = 0.925$ which is close to 1. Figure 2 shows that the exponential law (4) captures well the overall dependency of TMAC in terms of temperature T, although in some temperature range, the power law may perform better.

At high temperature range ($T > 350$ K), α_t reaches the almost constant and very small value of $\alpha_\infty = 0.0425$ as mentioned previously, the collisions are nearly elastic and specular. In the intermediate temperature region (50 K $< T <$ 200 K $\approx 4T_0$), α_t increases with a higher rate owing to the exponential behavior revealing the increase of the adsorption contribution. In the small temperature region ($T < 50$ K $\approx T_0$), the adsorption is the dominant mechanism in the collision process.

We note that in literature works on the dependency of TMAC on temperature, the property (5) is not always observed. For example, for the couple Ar/Pt in different simulation conditions, we found $\alpha_\infty + \alpha_0 = 0.5$ ($\alpha_\infty = 0.32$ and $\alpha_0 = 0.17$ with $T_0 = 115$ K) for T ranging from 100 K to 400 K in Ref [40], $\alpha_\infty = 0.25$ and $\alpha_0 = 0.75$ with $T_0 = 125$ K in Ref [41] and $\alpha_\infty = 0.065$ and $\alpha_0 = 1.055$ with $T_0 = 588$ K in Ref [42] for T ranging from 200 K to 400 K. The reasons explaining the large variation of the parameters value are: the small temperature range investigated and the TMAC computation methodology (Couette flow with Ar/Ar interaction in Ref [40], collisionnal method with rigid surface in Ref [41], collisionnal method with one incident angle in Ref [42]). The work of Reynold et al. [41] gives the more coherent results

with the respect to ours especially about the constraint Eq.(5) presumably because their methodology is close to ours. In Ref. [42], the authors found an important adsorption contribution even at room temperature (TMAC = 0.64 at $T = 350$ K) which leads to a very high value of T_0 compared to the two others.

2.3. Resident time and surface diffusion

From the distribution of resident time, we can find significant difference between hot and cold surface (see Fig. 4). For hot surface at $T = 350$ K, the reflection is quasi instantaneous, corresponding short resident time with the peak at 1.4 ps. The fraction of resident time longer than 20-25 ps are small and associated to collision and reflection at large incident angle and small vertical velocity $v_z, v'_z \simeq 0$. The resident time distribution agrees well with the Frechet (inverse Weibull) distribution

$$\mathrm{Fr}(\beta, 0, \tau_\beta) = \frac{\beta}{\tau_\beta}\left(\frac{\tau_\beta}{\tau}\right)^{\beta+1} \exp\left[-\left(\frac{\tau_\beta}{\tau}\right)^{\beta}\right], \quad \beta > 0 \tag{6}$$

and less well with the exponential distribution

$$\mathrm{Exp}(0, \tau_\beta) = \frac{1}{\tau_\beta} \exp\left[-\frac{\tau}{\tau_\beta}\right] \tag{7}$$

We note that if wall force is neglected, the atom travelling is ballistic within a fixed vertical distance δ_z and the distribution of the incident velocity v_z is the Rayleigh distribution $v_z \sim \mathcal{R}(\sqrt{k_B T/m_{He}})$, the exact residence time distribution $\tau = \delta_z/v_z$ is the Frechet distribution $\tau \sim \mathrm{Fr}(2, 0, h/\sqrt{2k_B T/m_{He}})$. Taking $\delta_z = 2r_{cut} - \sigma_{HeC}$ which includes both incident and bouncing distance, we find the mode of the Frechet distribution is at 1.4 ps, which is the value found from the MD histogram. However, although the Frechet distribution captures overall allure of the histogram, the long time power law of the Frechet distribution overestimates the tail which decreases at faster rate.

In contrast, for cold surface $T = 50$ K, the most probable resident time and displacement is 4 ps but long resident time events are no longer restricted to small normal velocity but spread over a large range of velocity. Both Frechet and exponential distribution only can not describe the resident time. This suggests that the atom may be adsorbed at the surface and stay longer before desorped. As a result, the collision can be divided into two regimes: short resident time regime and a long plateau resident time regime. The former is associated to quasi instantaneous and ballistic reflection and the latter is associated to complex mechanism involving adsorption, surface diffusion and desorption. For the latter, atoms interact a lot with the wall and forget the initial incident velocity. To study further detail, we consider the velocity correlation of atoms staying at least certain duration called minimal resident time. Using 35 ps as cutoff limit to separate the collision data, we find that the collisions under 35 ps accounting for roughly 64% of population are strongly correlated as $\rho_{v_x v'_x} = 0.80$ and those over 35 ps is very weakly correlated $\rho_{v_x v'_x} = 0.06$, which is close to diffusive behavior. Later study show that the full diffusive behavior starts at around 70 ps where $\rho_{v_x v'_x} \simeq 0$ and the ballistic behavior ends at 20-25 ps.

Inspecting the two populations associated to two regimes, we find that the distribution of tangential velocity v_x is less sensitive to this division and can be approximated as Maxwell equilibrium distribution (see Fig. 5). This means that both long and short resident time are equally present for the whole range of v_x. The distribution of normal velocity v_z is more sensitive to the division. Compared with the equilibrium distribution, the overshoot in small velocity range and undershoot in large velocity range shows that smaller normal velocities are more likely to be associated with long resident time and vice versa. Next let us look at the square displacement of atoms during the resident time at 50 K as displayed Fig. 6. We find that the displacement can be as far as 2000 Å especially for atoms staying long time near the surface.

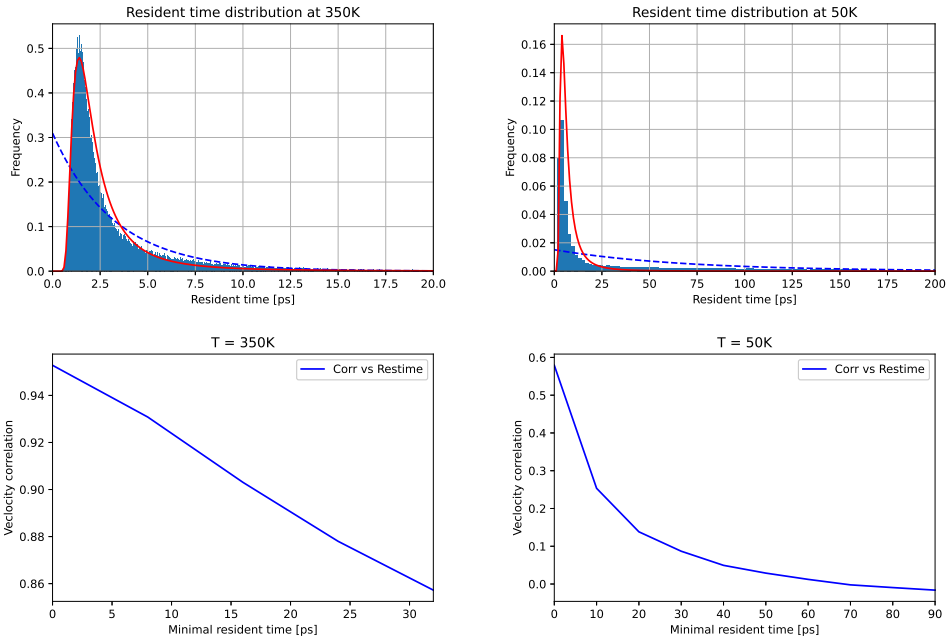

Figure 4: Top: Resident time and displacement distribution at 350 K and 50 K. Dashed lines represent exponential pdf fit $\mathrm{Exp}(0, \tau_\beta)$ with τ_β being characteristic waiting time and solid lines Frechet pdf (inverse Weibull) fit $\mathrm{Fr}(2, 0, \tau_\beta)$. Bottom: correlation coefficient of post and pre collision velocity of atoms as function of minimal resident time.

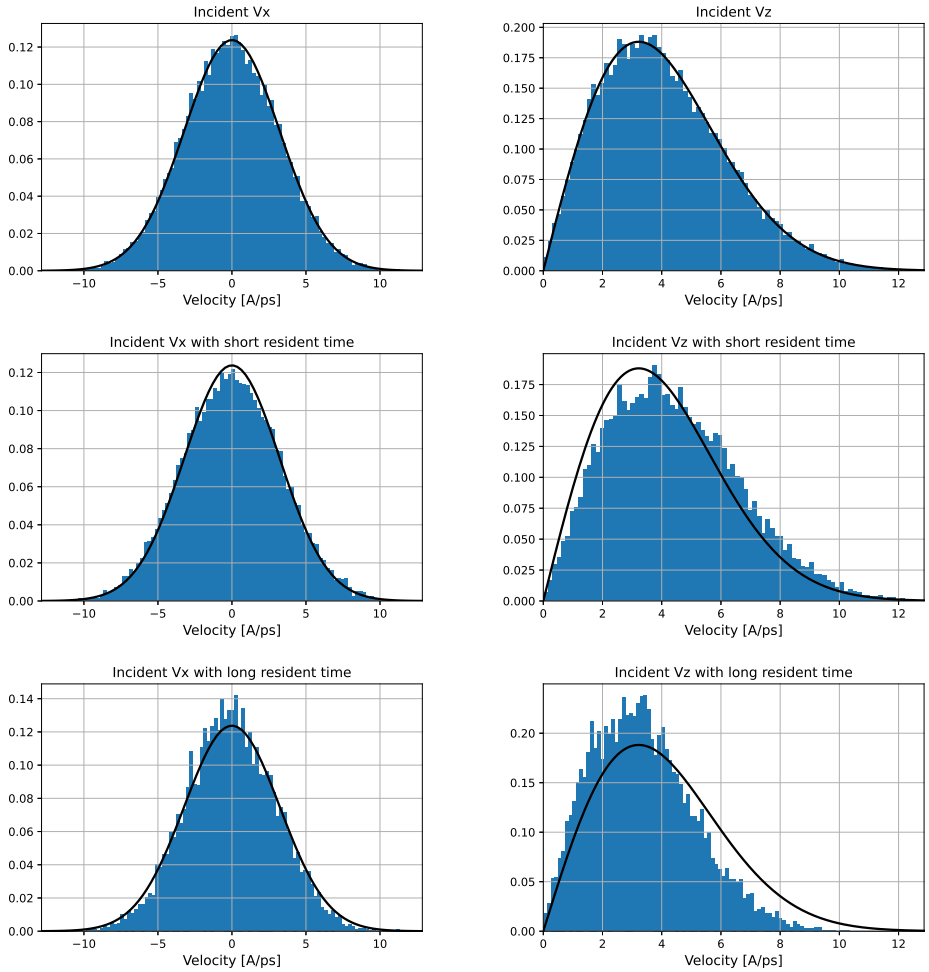

Figure 5: Distribution of incoming velocity at 50 K. Top left: Velocity v_x. Top right: Velocity v_z . Center left: Velocity v_x with short resident time ($<$ 35 ps). Center right: Velocity v_z with short resident time ($<$ 35 ps). Bottom left: Velocity v_x with long resident time ($>$ 35 ps). Bottom right: Velocity v_z with long resident time ($>$ 35 ps). Solid lines correspond to equilibrium distribution at $T = 50$ K: Maxwellian for v_x and Rayleighian for v_z

To quantify the surface diffusion effect, we divide the resident time into small intervals Δt and compute approximately the average square displacement in the interval with the formula:

$$\mathrm{MSD}(t) \simeq \langle x^2(t') + y^2(t') \rangle_{t' \in [t-\Delta t/2 \; t+\Delta t/2]} \tag{8}$$

In the range $0 - 20$ ps, we can find a parabolic ballistic regime where $\mathrm{MSD}(t) \propto t^2$. After a transition $20 - 60$ ps, the MSD changes curvature and enter the linear diffusive regime $\mathrm{MSD}(t) \propto t$. This linear regime is observed upto 500 ps with the slope of 1155 Å^2/ps, which corresponds to a surface diffusivity of $D_s = 289$ Å^2/ps. The diffusion behavior corresponds to weak energy barrier-low friction diffusion regime [33]. Indeed, the value of e^{-E_a/k_BT} is close to 1 with the activation energy $E_a = 0.0014$ eV (16 K) and the friction coefficient $\eta = 2k_BT/(m_{He}D_s) = 0.074$ ps^{-1} is much lower than the reference value $\sqrt{k_BT/(m_{He}a^2)} = 1.31$ ps^{-1} using the lattice spacing of graphene $a = 2.46$ Å. The coefficient $1/\eta = 13.5$ ps is also the timescale of the parabolic stage. This behavior is completely different from the behavior at 350 K where the ballistic regime is found for most of the collision.

When the atoms enter the surface diffusion regime, the input velocity is forgotten, noted by zero correlation between input and the output velocity. The existence and extent of surface diffusion is thus governed by the temperature. From Fig. 8, we find that, the diffusion regime seems to exist at temperature as low as 50 K and 75 K, for a significant number of atoms staying more than 90 ps near the surface. However as the temperature increases, the surface diffusion seems to disappear, i.e the atoms is desorbed before truly entering the diffusion regime. The loglog plot of MSD vs time also confirm this remark. The graphic at 50 K and 75 K is composed of two slopes $\mathrm{MSD} \propto t^2$ and $\mathrm{MSD} \propto t$ corresponding to ballistic and fully developed diffusive regime. The transition to fully developed diffusive regime is around 60 ps at 50 K and 100 ps at 75K. At other temperatures, there is almost no surface diffusion.

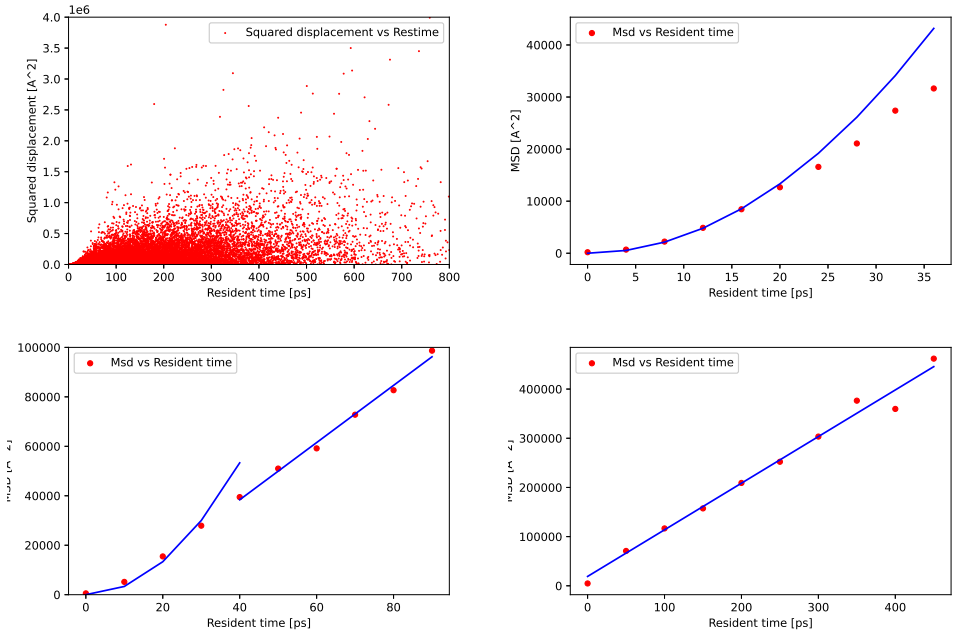

Figure 6: Analysis of surface MSD at 50K. Top left: Surface square displacement of all atoms during the resident time. Top right: Mean square displacement and resident time in range 0-40 ps with parabola fit. Bottom left: Mean square displacement and resident time in range 0-100 ps with parabola for short time and linear fit for long time. Bottom right: Mean square displacement and resident time in range 0-500 ps with linear fit.

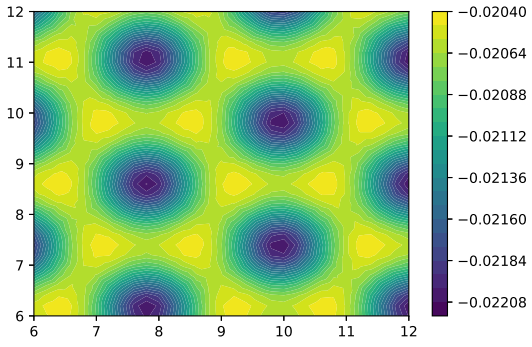

Figure 7: Potential energy surface (unit eV). The energy barrier $E_a \simeq 0.0014$ eV or $E_a/k_B \simeq 16$ K

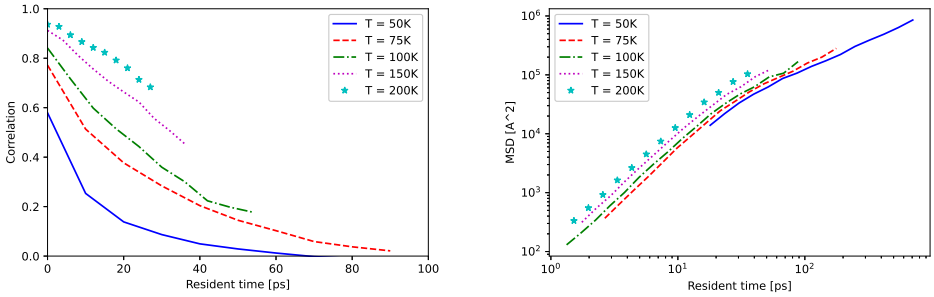

Figure 8: Left: Correlation coefficient of post and pre collision velocity of atoms as function of minimal resident time. Right: Mean square displacement as function of resident time at different temperature

3. Self diffusion of dilute Helium gas in nano graphitic channel

The self diffusion simulations are performed in a channel composed of two graphitic walls of the same dimensions as in the collision simulations. The investigation is carried out for two channel widths $d_W = 34$ Å, 50 Å, which is the distance between the two surface atomic planes. The gas is considered dilute so that, the interaction between each Helium atoms and the wall is treated independently. That condition will render the gas transport close to Knudsen diffusion. However, as we will see later, the Knudsen diffusion is not sufficient to describe the complex transport phenomenon in the nano channel. Using MD simulations, we study 600-1200 trajectories of He atoms in the graphite channel during 100 ns with a temperature ranging from 50 K and 700 K. After equilbration step, we compute the mean square displacement (MSD) of the atoms as function of time t and the self-diffusion coefficient by the relation

$$\mathrm{MSD}(t) = \langle (\boldsymbol{r}(t) - \boldsymbol{r}(0))^2 \rangle, \quad D = \lim_{t\to\infty} \frac{\partial}{4\partial t} \mathrm{MSD}(t) \tag{9}$$

where $\boldsymbol{r}(t)$ (components $x(t), y(t)$) and $\boldsymbol{r}(0)$ (components $x(0), y(0)$) are the planar position vectors of the atoms at time t and 0 respectively. This limit expression is observed in the case of normal diffusion. Otherwise, the dif-

fusion falls into anomalous diffusion depending on how MSD(t) varies with t. For example, if MSD(t) $\propto t^{\alpha}$ at long time range, then $\alpha < 1$ for sub-diffusion or $\alpha > 1$ for superdiffusion. In these cases, D should be defined as instantaneous diffusion coefficient $D(t)$ at time t or an effective diffusion coefficient for a given time range [59, 60]. Random walk simulations based on stochastic gas wall collision model with parameters determined from MD collision data in Section 2 are also done under the same physics conditions and diffusivity results issued from MSD will be compared with MD simulations of self diffusion. Regarding theoretical results in relation with the same system, Arya et al. [27] used a stochastic model without waiting time to estimate the Knudsen diffusivity at infinite time limit. In order to obtain a finite diffusivity, a cutoff velocity v_C was introduced. It can be deduced that the velocity v_C is related to the time range to compute the diffusivity mentioned above as small velocity-long flying time events are not counted in the time range. In order to compare with the Arya formula, we use a fixed cutoff time $\tau_C = h/v_C$ which is more directly connected to the time range under consideration. The details of will be presented in the following.

3.1. Comparison between MD and stochastic simulations based on gas-wall scattering models

The stochastic approach consists in considering the particle trajectories as a series of free flights between two collisions with two parallel walls. No interaction is assumed between the wall and the particles. In the present work, the random walk simulations are performed in a 2D geometry. The total number of particles is 10^3 and each particle will have 10^5 collisions. Whenever a particle collides with any of the two wall, its time and position are recorded. It is also given a new post collision velocity which depends on the pre collision velocity and if the surface displacement $(\Delta x)_{surf}$ and waiting time t_w is accounted, the position and timestamp are modified accordingly (see Fig. 9). The details of the collision model will be given further below. All this information constitutes the trajectory of the particle. Next, to sample

the displacement $\Delta x(t)$ at fixed time t, the starting time t_{start} is chosen randomly and the positions $x(t_{start})$ at t_{start} and $x(t_{end})$ at the ending time $t_{end} = t_{start} + t$ are interpolated from two nearest collision points in the above trajectory. The displacement is then calculated from the difference of positions between t_{start} and t_{end}, i.e $\Delta x(t) = x(t_{end}) - x(t_{start})$. To achieve good statistics, about 10^3 samples are collected for each trajectory.

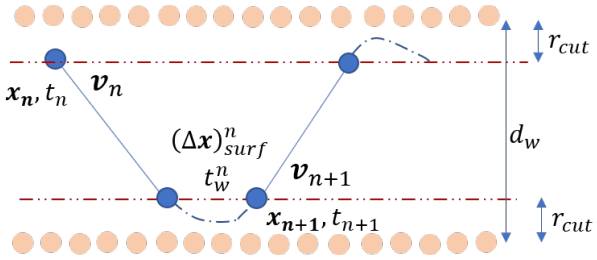

Figure 9: Sketch of stochastic simulation for Knudsen diffusion in nanopore (bottom).

Let us consider first the CL scattering model [26] without waiting time and surface displacement $t_w = 0$ and $(\Delta x)_{surf} = 0$. From the correlation of the incoming and outgoing velocity, we can construct the stochastic relation. Given pre collision velocity v_x, the post collision velocity v'_x is given by the formula

$$v'_x = (1 - \alpha_t)v_x + \sqrt{\alpha_t(2 - \alpha_t)}v_x^M, \quad v_z = v_z^R \tag{10}$$

where v_x^M and v_z^R are random variables drawn from the normal and Rayleigh distribution at the same temperature

$$v_x^M \sim \mathcal{N}(0, \sqrt{k_B T/m_{He}}), \quad v_z^R \sim \mathcal{R}(\sqrt{k_B T/m_{He}}) \tag{11}$$

We have shown that the normal and the tangential scattering processes are not correlated. This justifies the separation of the normal and tangential scattering components. But, even if Fig. 2 shows a smaller specular contribution, the diffusive scattering of the normal velocity component is not

rigorously observed. Assuming that the surface is isotropic, the velocity and motion along the y direction is modelled the same way as the x direction. Thus for the brevity of the paper, we only mention the direction x from now on.

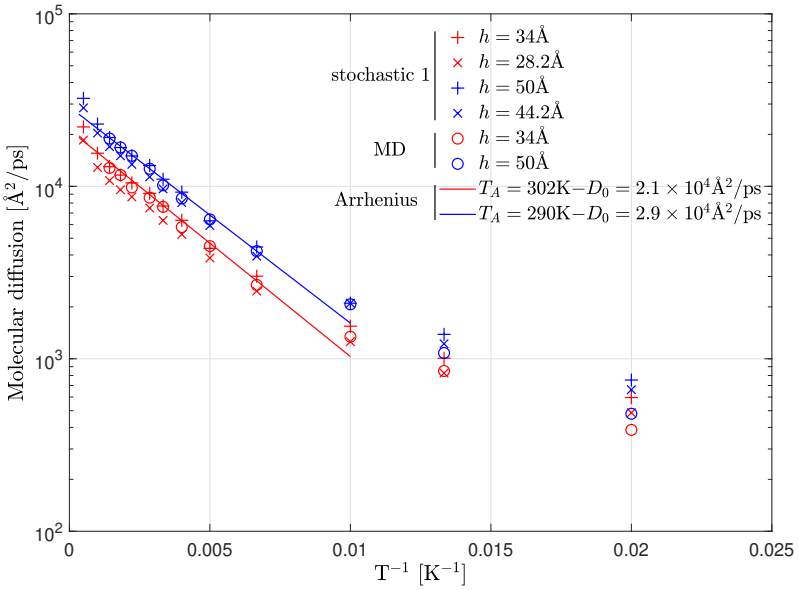

Figure 10: Molecular diffusion vs. $1/T$. Comparison between molecular dynamics ($\circ$) and the 1^{st} ($\times$,$+$) and the 2^{nd} ($*$) stochastic methodologies (without and with surface diffusion). Solid lines: Arrhenius law $D = D_0 e^{-T_a/T}$. The stochastic simulations are performed with the TMAC calculated by molecular dynamics and with the paramters gathered in Table 1 in the case of the 2^{nd} methodology.

Figure 10 shows the variation of the diffusion coefficients with respect to the inverse of temperature for the two wall distances d_W. Regarding the stochastic simulations, we use two distances $h = d_W$ (34 Å and 50 Å) and $h = d_W^{eff} \approx d_W - 2\sigma_{HeC}$ (28.2 Å and 44.2 Å) as suggested by Ref. [27] in which the excluded volume effect of hard sphere model is taken into account. We find that in the temperature range 100 K $< T <$ 1000 K, the diffusion coefficients can be approximated by Arrhenius law with a characteristic temperature

$T_A \simeq 300$ K:

$$D(T) = D_0 e^{-T_A/T} \tag{12}$$

T_A is little sensitive to d_W and D_0 is proportional to the slit width. In lower temperature range $T < 100$ K or higher temperature range $T > 1000$ k, the deviation from Arrhenius law is significant.

The stochastic results for both $h = d_W$ and $h = d_W^{eff}$ are close to each other for all temperature and close to the MD results in high temperature range ($T > 100K$). Qualitatively speaking, the MD results lie between the stochastic results with $h = d_W$ and $h = d_W^{eff}$ being the upper and lower bounds respectively. With larger channel width $h = 50$Å, the surface effect is reduced and the MD results and stochastic results associated to $h = d_W$ and $h = d_W^{eff}$ nearly coincides. However, in small temperature range ($T < 100K$), the difference between the stochastic and MD results is increasingly observable. Especially at 50 K, the stochastic models overestimate upto 40 %, with respect to MD results. The difference is mainly due to the adsorption and surface diffusion which are seen in MD simulations but are not taken into account in the stochastic models. This motivates us to improve the stochastic models to capture both adsorption and surface diffusion, as illustrated in Fig. 11 and described in details as follow.
At low temperatures 50 K-75 K, both short and long reflection exists with portion w and $1-w$ respectively, with transition time τ_{tr} as threshold value. The latter corresponds to the moment when diffusive regime is fully developed and the velocity correlation is equal to zero (see Fig. 8), $\tau_{tr} = 60$ ps at 50 K and 100 ps at 75K. The waiting time for each types $t_{ws} \leq \tau_{tr}$ and $t_{wl} \geq \tau_{tr}$ is modelled by Frechet and exponential distributions with different location and scale parameters

$$t_{ws} \sim \mathrm{Fr}(2, 0, \tau_s), \quad t_{wl} \sim \mathrm{Exp}(\tau_{tr}, \tau_l) \tag{13}$$

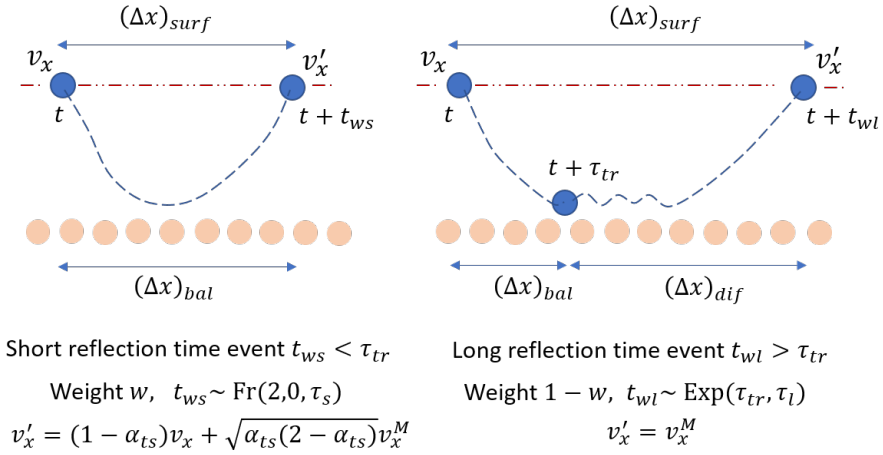

Figure 11: Sketch of stochastic collision model for short (left) and long (right) reflection time events at 50K et 75K. At higher temperatures, the reflection is mostly short time and only short reflection model is used.

Since the support of $\mathrm{Fr}(2,0,\tau_s)$ is $(0,\infty)$, when generating t_{ws} from the distribution, only values smaller than τ_{tr} are utilized.

For short time reflection, it is relevant to consider that surface velocity v_{sx} of atoms approximately constant and close to the average of incident and reflected velocity v_{mx}

$$v_{sx} = \frac{(\Delta x)_{surf}}{\Delta t}, \quad v_{mx} = \frac{1}{2}(v_x + v'_x), \quad v_{sx} \simeq v_{mx} \tag{14}$$

and v'_x is determined from v_x via CL model with accommodation coefficients α_{ts} like (10). As a result, the ballistic displacement of the atom during the waiting time t_w is given by

$$(\Delta x)_{surf} = v_{mx} t_{ws} \tag{15}$$

For long reflection time atom $t_{wl} \geq \tau_{tr}$, the surface motion of atoms is composed of ballistic regime $(\Delta x)_{bal}$ with average velocity v_{mx}, the intermediate

regime and diffusive regime $(\Delta x)_{dif}$ with diffusion coefficient D_s. Since the behavior of the intermediate regime is generally unknown, to the first order of approximation, we consider that there are only two ballistic and diffusive regimes separated by transition time τ_{tr}. Consequently we have,

$$(\Delta x)_{surf} = (\Delta x)_{bal} + (\Delta x)_{dif} \tag{16}$$

with the ballistic process before τ_{tr}

$$(\Delta x)_{bal} = \tau_{tr} v_{mx}, \quad v_{mx} = \frac{1}{2}(v_x + v_x^M), \quad v_x^M \sim \mathcal{N}(0, \sqrt{k_B T/m_{He}}) \tag{17}$$

and the diffusive process starting after τ_{tr}

$$(\Delta x)_{dif} \sim \mathcal{N}(0, \sqrt{2D_s(t_{wl} - \tau_{tr})}) \tag{18}$$

T K	τ_{tr} [ps]	w	τ_s [ps]	τ_l [ps]	α_{ts} [ps]	D_s [Å^2/ps]
50	60	0.70	4.157	140	0.23	289
75	100	0.97	3.79	39.66	0.21	401

Table 1: Parameters of stochastic wall models with surface diffusion.

The waiting time and the surface diffusion coefficient are computed with the TMAC computation method described above. While the transition time τ_{tr} is determined from the MSD curve (Fig. 8), the two parameters τ_s and τ_l are determined by fitting the residence time distribution with probability law by maximum likelihood estimation method based on Eq. (13). All the parameters of the gas wall stochastic model are given in Table 1. To be consistent with the construction of wall model, the free flight takes place over a width of $d_W - 2r_{cut}$. For the two slit widths, we can find that the new stochastic results are close to the MD results at 50 and 75K, as shown in Table 2. This effect confirms the importance of the simulation that includes the surface diffusion effect.

T [K]	Self diffusivity [Å^2/ps]							
	$d_W = 34$ Å				$d_W = 50$ Å			
	MD	Stoch 1 d_W	Stoch 1 d_W^{eff}	Stoch 2	MD	Stoch 1 d_W	Stoch 1 d_W^{eff}	Stoch 2
75	850	1008	826	713	1080	1386	1222	1040
50	387	596	487	317	480	753	662	386

Table 2: Comparison of two stochastic simulations with MD results at 50K and 75K

We want to highlight the fact that at 50K, only combining both short and long reflection time regimes in the stochastic model as described above can we obtain the diffusion coefficient of the same order as MD simulations. Considering all reflection as short time will overestimate and all reflection as long time as Ref. [61] will underestimate the diffusion coefficient.

3.2. Comparison between MD and theoretical estimation

Arya et al. [27] extended the Smoluchowski model [25] by using the scattering model formulated by Eqs. (10) and (11). We have to recall that in these models the walls are rigid, i.e the wall temperature is not defined, the particle/wall interaction is modeled by the hard sphere potential.

In order to derive an analytic expression of the Knudsen diffusion, the tangential velocity after n collisions is first obtained as function of $n-1$ previous tangential velocities and random diffuse velocities associated to the thermal stochastic wall. Under the assumption that the diffuse velocities are uncorrelated to the reflected velocity, the gas phase is in thermodynamic equilibrium and the free flight time between each collision events is independent, the diffusion coefficient for an infinite number of wall collisions has the following expression:

$$D_{Arya} = \frac{\langle v_x^2 \rangle \langle \tau^2 \rangle}{\langle \tau \rangle} \left[1 + 2 \frac{\langle \tau \rangle^2}{\langle \tau^2 \rangle} \frac{(1-\alpha_t)}{\alpha_t} \right] \tag{19}$$

where τ is the free flight time over the slit width and $\langle\rangle$ is the average over the Maxwell-Boltzmann distribution. However, the integral of the term $\langle\tau^2\rangle$ converges only if the velocity is truncated ($v_x > v_C$ where v_C is the cutoff velocity). The final expression of D_{Arya} is:

$$D_{Arya} = -h\sqrt{\frac{\pi k_B T}{2m}}\left[\frac{\ln\epsilon}{2\pi} - \frac{(1-\alpha_t)}{\alpha_t}\right] \tag{20}$$

where $\epsilon = (mv_C^2)/(2k_BT)$ and $h = d_W$ or d_W^{eff}. The logarithmic dependence on ϵ shows that D_{Arya} is little sensitive to the truncation. To compare with the Ayria formula from MD results, we consider a fixed cut off time τ_C of order ns which is comparable to MD duration 100 ns. Like v_C, τ_C is an empirical coefficient which is related to v_C via the relation $\tau_C = h/v_C$. We shall investigate how well the analytical expression can fit with the MD results by varying τ_C from 10 ns to 100 ns.

Using the TMAC values determined by MD and $h = d_W$, Fig. 12 shows that D_{Arya}, which is not sensitive to τ_C lying between 10 ns and 100 ns agrees with the diffusion coefficient computed by MD in the Arrhenius region for the two wall distances 34 Å and 50 Å. The maximum relative difference from MD results in this temperature range is of order 5% for small channel case $h = 34$ Å and 10% for large channel case $h = 50$ Å. This confirms the observation made in section 3.1 and the limits of the TMAC relevance. In the Arya model, the diffuse collision is only controlled by the surface roughness. So, for the same reason invoked for the stochastic model, the adsorption effect tends to reduce the diffusion coefficient and $D_{Arya} > D_{MD}$ at small temperature. At lower temperature range, D_{Arya} is more sensitive to τ_C and the difference from MD results are larger. We find that using $\tau_C = 10$ ns yields smaller error than $\tau_C = 100$ ns. At 50K and $h = 50$ Å for example, the error of $\tau_C = 10$ ns is 50% compared with 81 % when $\tau_C = 100$ ns.

The behavior D_{Arya} could be seen as the results of the expression of $\alpha_t(T)$ in temperature (4) and $\sqrt{T}$ coming from (20). If we neglect the first term

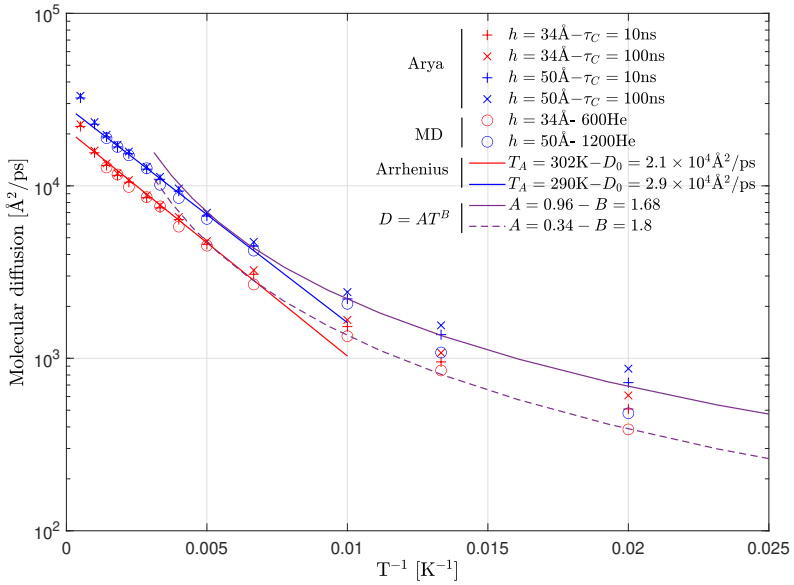

Figure 12: Molecular diffusion vs. 1/T. Comparison between the Arya model (×,+) and the MD simulations (∘). Blue and red solid lines: Arrhenius law $D = D_0 e^{-T_A/T}$. Purple lines: power law curves. The Arya model is calculated with the TMAC determined by molecular dynamics and with $h = d_W$ with two cutoff times τ_C: 10 ns and 100 ns.

$\ln \epsilon/2\pi \simeq -2.5 \ll (1-\alpha_t)/\alpha_t$ in (20) at sufficiently high temperature and use (4) and (5), the temperature dependency of diffusivity D is through the temperature function $F(T)$, $D \propto F(T)$ with $F(T) = \sqrt{T}\frac{1-\alpha_t(T)}{\alpha_t(T)}$. In the intermediate temperature range 150K-1000K, it can be approximated by the Arrhenius law (12) but the deviation from the Arrhenius law is clearer at higher temperature $T > 1000$K as $F(T) \propto \sqrt{T}$. This is due to the fact that above 450 K, the accommodation coefficient α_t becomes constant. At lower temperature range $50 - 150$K, both the two terms $\ln \epsilon/2\pi$ and $\frac{1-\alpha_t(T)}{\alpha_t(T)}$ are comparable resulting a power law behavior $D_{Arya} \propto T^{1.68}$ compared to the MD data $D_{MD} \propto T^{1.8}$. The equation (20) also suggests that at very low temperature, for example $T < 50$K, where α_t close to 1 and $\ln \epsilon/2\pi \gg \frac{1-\alpha_t(T)}{\alpha_t(T)}$ and $D_{Arya} \propto \sqrt{T} \ln \epsilon$. However, at such low temperature, the MD simulations show that the adsorption is dominant and the equation (20) can be erroneous.

4. Conclusion

In the present paper, we use Molecular Dynamics and stochastic modelling and simulations to investigate the collisions of Helium on graphite surface and the self diffusion of Helium in graphite nanochannel. The main findings are the following

- The collisions of Helium on graphite surface are simulated by MD. At high temperature, the TMAC coefficient is very small and the reflection is mostly short time. Although the reflection is not truly specular, the pre and post tangential velocities are strongly correlated. However at low temperature, especially at 50K and 75K, the correlation is weakened and there are both short and long time reflections. We observe adsorption and surface diffusion for the long time reflection events. The latter corresponds to weak energy barrier-low friction diffusion regime. The surface diffusivity is quantified by MSD of surface displacement.
- A stochastic model for gas wall interaction is constructed. The model includes both short and long time reflection with associated waiting time and surface displacement. For long time reflection, the surface displacement is composed by a ballistic displacement followed by a diffusive displacement. For short time reflection, only ballistic displacement is adopted. The parameters of the stochastic model are identified from MD collision data.
- We simulate the self diffusion of Helium in graphite channels by Molecular Dynamics and by Random Walk (RW) methods. The RW method is based on the gas-wall stochastic models developed earlier. It is found that at high temperature, the RW without waiting time and surface displacement agree with the MD results. However at low temperature, only RW with waiting time and surface displacement produce good diffusivity coefficient. We emphasize that both short time and long time reflection must be included, otherwise the diffusivity will be under or overestimated by RW simulations. We also found that the Arrhenius empirical law can represents that diffusivity temperature relation at high temperature.

- The numerical results are compared with theoretical results from Ref. [27] based. A cutoff time τ_C related to cutoff velocity v_C allows to calibrate analytical formula with MD results. It is found that the theoretical formula gives good approximation at high temperature but the accuracy becomes worse at low temperature. We deduce that the failure of theoretical formula is due to the waiting time and the surface displacement originating from adsorption and surface diffusion phenomenon are not taken into account.

The present paper does not only provide interesting results concerning the collision and the self diffusion of He and graphite but also a general multi stage framework coupling Molecular Dynamics and stochastic simulation to study the gas diffusion nanoporous material.

Declaration of Competing Interest

The authors declare that they have no known competing financial interests or personal relationships that could have appeared to influence the work reported in this paper.

Ackowledgments

Centre de Calcul Intensif d'Aix-Marseille is acknowledged for granting access to its high performance computing resources.

References

[1] Z. Xiao, L. B. Kong, S. Ruan, X. Li, S. Yu, X. Li, Y. Jiang, Z. Yao, S. Ye, C. Wang, et al., Recent development in nanocarbon materials for gas sensor applications, Sens. Actuators B Chem. 274 (2018) 235–267.

[2] C. R. Minitha, V. S. Anithaa, V. Subramaniam, R. T. Rajendra Kumar, Impact of oxygen functional groups on reduced graphene oxide-based

sensors for ammonia and toluene detection at room temperature, ACS Omega 3 (4) (2018) 4105–4112.

[3] J. H. Choi, J. Lee, M. Byeon, T. E. Hong, H. Park, C. Y. Lee, Graphene-based gas sensors with high sensitivity and minimal sensor-to-sensor variation, ACS Appl. Nano Mater. 3 (3) (2020) 2257–2265.

[4] I. C. Gerber, P. Serp, A theory/experience description of support effects in carbon-supported catalysts, Chem. Rev. 120 (2) (2019) 1250–1349.

[5] N. Talukder, Y. Wang, B. B. Nunna, E. S. Lee, Nitrogen-doped graphene nanomaterials for electrochemical catalysis/reactions: A review on chemical structures and stability, Carbon 185 (2021) 198–214.

[6] S. K. Alen, S. Nam, S. A. Dastgheib, Recent advances in graphene oxide membranes for gas separation applications, Int. J. Mol. Sci. 20 (22) (2019) 5609.

[7] J. S. Adams, A. K. Itta, C. Zhang, G. B. Wenz, O. Sanyal, W. J. Koros, New insights into structural evolution in carbon molecular sieve membranes during pyrolysis, Carbon 141 (2019) 238–246.

[8] X. He, L. Lei, Z. Dai, Green hydrogen enrichment with carbon membrane processes: Techno-economic feasibility and sensitivity analysis, Sep. Purif. Technol. 276 (2021) 119346.

[9] H. Su, Y. H. Hu, Recent advances in graphene-based materials for fuel cell applications, Energy Sci. Eng. 9 (7) (2021) 958–983.

[10] D. Sui, M. Wu, K. Shi, C. Li, J. Lang, Y. Yang, X. Zhang, X. Yan, Y. Chen, Recent progress of cathode materials for aqueous zinc-ion capacitors: Carbon-based materials and beyond, Carbon 185 (2021) 126–151.

[11] F. Yang, J. Gu, L. Ye, Z. Zhang, G. Rao, Y. Liang, K. Wen, J. Zhao, J. B. Goodenough, W. He, Justifying the significance of knudsen diffusion in solid oxide fuel cells, Energy 95 (2016) 242–246.

[12] S. Salari, M. Tam, C. McCague, J. Stumper, M. Bahrami, The ex-situ and in-situ gas diffusivities of polymer electrolyte membrane fuel cell catalyst layer and contribution of primary pores, secondary pores, ionomer and water to the total oxygen diffusion resistance, J. Power Sources 449 (2020) 227479.

[13] L. Zhang, C. Liu, Q. Li, S. Wang, S. Cai, E. Huo, Shale gas transport through the inorganic cylindrical and conical nanopores: A density gradient driven molecular dynamics, Int. J. Heat Mass Transf. 183 (2022) 122126.

[14] D. Feng, Z. Chen, K. Wu, J. Li, X. Dong, Y. Peng, X. Jia, X. Li, D. Wang, A comprehensive review on the flow behaviour in shale gas reservoirs: Multi-scale, multi-phase, and multi-physics, Can. J. Chem. Eng. 100 (11) (2022) 3084–3122.

[15] H. Wang, L. Chen, Z. Qu, Y. Yin, Q. Kang, B. Yu, W.-Q. Tao, Modeling of multi-scale transport phenomena in shale gas production — a critical review, Applied Energy 262 (2020) 114575.

[16] C. A. Scholes, U. K. Ghosh, Review of membranes for helium separation and purification, Membranes 7 (1) (2017) 9.

[17] Z. Dai, J. Deng, X. He, C. A. Scholes, X. Jiang, B. Wang, H. Guo, Y. Ma, L. Deng, Helium separation using membrane technology: recent advances and perspectives, Sep. Purif. Technol. 274 (2021) 119044.

[18] F. Li, Y. Qu, M. Zhao, Efficient helium separation of graphitic carbon nitride membrane, Carbon 95 (2015) 51–57.

[19] J. Lee, J. H. Kim, Statistical assessment of tangential momentum accommodation coefficient using internal flow rate model based on rarefied gas conditions, Results Phys. 43 (2022) 106130.

[20] J.-J. Shu, J. Bin Melvin Teo, W. Kong Chan, Fluid Velocity Slip and Temperature Jump at a Solid Surface, Appl. Mech. Rev. 69 (2) (2017).

[21] D. Bayer-Buhr, M. Vimal, A. Prakash, U. Gross, T. Fieback, Determination of thermal accommodation coefficients on casio3 and sio2 using molecular dynamics and experiments, Int. J. Heat Mass Transf. 183 (2022) 122219.

[22] T. Sipkens, K. Daun, Using cube models to understand trends in thermal accommodation coefficients at high surface temperatures, Int. J. Heat Mass Transf. 111 (2017) 54–64.

[23] J. C. Maxwell, Vii. on stresses in rarified gases arising from inequalities of temperature, Philos. Trans. R. Soc. (170) (1879) 231–256.

[24] M. Knudsen, Die gesetze der molekularströmung und der inneren reibungsströmung der gase durch röhren, Ann. Phys. (Berl.) 333 (1) (1909) 75–130.

[25] M. Smoluchowski, Zur kinetischen theorie der transpiration und diffusion verdünnter gase, Ann. Phys. (Berl.) 338 (16) (1910) 1559–1570.

[26] C. Cercignani, M. Lampis, Kinetic models for gas-surface interactions, Transp Theory Stat Phys. 1 (2) (1971) 101–114.

[27] G. Arya, H.-C. Chang, E. J. Maginn, Knudsen diffusivity of a hard sphere in a rough slit pore, Phys. Rev. Lett. 91 (2) (2003) 026102.

[28] T. Liang, Q. Li, W. Ye, A physical-based gas–surface interaction model for rarefied gas flow simulation, J. Comput. Phys. 352 (2018) 105–122.

[29] T. Liang, Q. Li, Accurate modeling of knudsen diffusion in nanopores using a physical-based boundary model, J. Appl. Phys. 126 (8) (2019) 084304.

[30] N. Mateljevic, J. Kerwin, S. Roy, J. Schmidt, J. C. Tully, Accommodation of gases at rough surfaces, J. Phys. Chem. C 113 (6) (2009) 2360–2367.

[31] A. Filinov, M. Bonitz, D. Loffhagen, Microscopic modeling of gas-surface scattering. i. a combined molecular dynamics-rate equation approach, Plasma Sources Sci Technol. 27 (6) (2018) 064003.

[32] A. Filinov, M. Bonitz, D. Loffhagen, Microscopic modeling of gas-surface scattering: Ii. application to argon atom adsorption on a platinum (111) surface, Plasma Sources Sci Technol. 27 (6) (2018) 064002.

[33] T. Ala-Nissila, R. Ferrando, S. C. Ying, Collective and single particle diffusion on surfaces, Adv. Phys. 51 (3) (2002) 949–1078.

[34] J. V. Barth, Transport of adsorbates at metal surfaces: from thermal migration to hot precursors, Surf. Sci. Rep. 40 (3-5) (2000) 75–149.

[35] G. Antczak, G. Ehrlich, Jump processes in surface diffusion, Surf. Sci. Rep. 62 (2) (2007) 39–61.

[36] S. M. Mofidi, H. Nejat Pishkenari, M. R. Ejtehadi, A. V. Akimov, Role of graphene surface ripples and thermal vibrations in molecular dynamics of c60, J. Phys. Chem. C 123 (32) (2019) 20026–20036.

[37] H. Bulou, O. Lucas, M. Kibaly, C. Goyhenex, Long-time scale molecular dynamics study of co diffusion on the au (111) surface, Comput. Mater. Sci. 27 (1-2) (2003) 181–185.

[38] M. Jafary-Zadeh, C. D. Reddy, V. Sorkin, Y.-W. Zhang, Kinetic nanofriction: a mechanism transition from quasi-continuous to ballistic-like brownian regime, Nanoscale Res. Lett. 7 (1) (2012) 1–8.

[39] G. Karniadakis, A. Beskok, N. Aluru, Microflows and nanoflows: fundamentals and simulation, Vol. 29, Springer Science & Business Media, 2006.

[40] B.-Y. Cao, M. Chen, Z.-Y. Guo, Temperature dependence of the tangential momentum accommodation coefficient for gases, Appl. Phys. Lett. 86 (9) (2005) 091905.

[41] J. Reinhold, T. Veltzke, B. Wells, J. Schneider, F. Meierhofer, L. C. Ciacchi, A. Chaffee, J. Thöming, Molecular dynamics simulations on scattering of single ar, n2, and co2 molecules on realistic surfaces, Comput. Fluids 97 (2014) 31–39.

[42] T. T. Pham, Q. D. To, G. Lauriat, C. Léonard, V. Van Hoang, Effects of surface morphology and anisotropy on the tangential-momentum accommodation coefficient between pt (100) and ar, Phys. Rev. E 86 (5) (2012) 051201.

[43] J. Sun, Z.-X. Li, Two-dimensional molecular dynamic simulations on accommodation coefficients in nanochannels with various wall configurations, Comput. Fluids 39 (8) (2010) 1345–1352.

[44] J. Sun, Z.-X. Li, Three-dimensional molecular dynamic study on accommodation coefficients in rough nanochannels, Heat Transf. Eng. 32 (7-8) (2011) 658–666.

[45] A. M. Berezhkovskii, L. Dagdug, S. M. Bezrukov, Bulk-mediated surface transport in the presence of bias, J. Chem. Phys. 147 (1) (2017) 014103.

[46] D. S. Grebenkov, Paradigm shift in diffusion-mediated surface phenomena, Phys. Rev. Lett. 125 (2020) 078102.

[47] P. F. Zito, A. Caravella, A. Brunetti, E. Drioli, G. Barbieri, Discrimination among gas translation, surface and knudsen diffusion in permeation through zeolite membranes, J. Membr. Sci. 564 (2018) 166–173.

[48] H. Yu, J. Fan, J. Chen, Y. Zhu, H. Wu, Pressure-dependent transport characteristic of methane gas in slit nanopores, Int. J. Heat Mass Transf. 123 (2018) 657–667.

[49] C. Sun, M. Liu, B. Bai, Molecular simulations on graphene-based membranes, Carbon 153 (2019) 481–494.

[50] H. Sun, J. Yao, D. yan Fan, C. chen Wang, Z. xue Sun, Gas transport mode criteria in ultra-tight porous media, Int. J. Heat Mass Transf. 83 (2015) 192–199.

[51] A. M. Berezhkovskii, L. Dagdug, S. M. Bezrukov, A new approach to the problem of bulk-mediated surface diffusion, J. Chem. Phys. 143 (8) (2015) 084103.

[52] H. Sha, S. Zhang, R. Faller, Molecular investigation of gas adsorption, separation, and transport on carbon nanoscrolls: A combined grand canonical monte carlo and molecular dynamics study, Carbon 132 (2018) 401–410.

[53] W. A. Steele, The physical interaction of gases with crystalline solids: I. gas-solid energies and properties of isolated adsorbed atoms, Surf. Sci. 36 (1) (1973) 317–352.

[54] O. Talu, A. L. Myers, Reference potentials for adsorption of helium, argon, methane, and krypton in high-silica zeolites, Colloids Surf. A Physicochem. Eng. Asp. 187 (2001) 83–93.

[55] F. Siperstein, A. Myers, O. Talu, Long range corrections for computer simulations of adsorption, Molecular Physics 100 (13) (2002) 2025–2030.

[56] M. Liao, R. Grenier, Q.-D. To, M. P. de Lara-Castells, C. Leonard, Helium and argon interactions with gold surfaces: Ab initio-assisted determination of the he–au pairwise potential and its application to accommodation coefficient determination, The Journal of Physical Chemistry C 122 (26) (2018) 14606–14614.

[57] M. Liao, Q.-D. To, C. Léonard, V. Monchiet, Non-parametric wall model and methods of identifying boundary conditions for moments in gas flow equations, Physics of Fluids 30 (3) (2018) 032008.

[58] M. Liao, Q.-D. To, C. Léonard, W. Yang, Prediction of thermal conductance and friction coefficients at a solid-gas interface from statistical learning of collisions, Physical Review E 98 (4) (2018) 042104.

[59] J. Wu, K. M. Berland, Propagators and time-dependent diffusion coefficients for anomalous diffusion, Biophysical journal 95 (4) (2008) 2049–2052.

[60] M. V. Chubynsky, G. W. Slater, Diffusing diffusivity: a model for anomalous, yet brownian, diffusion, Physical review letters 113 (9) (2014) 098302.

[61] T. Hori, T. Kamino, Y. Yoshimoto, S. Takagi, I. Kinefuchi, Mutual influence of molecular diffusion in gas and surface phases, Physical Review E 97 (1) (2018) 013101.